Structure and Ligand Selection of Hemoglobin II from *Lucina pectinata*[*][S]

José A. Gavira[‡], Ana Camara-Artigas[§], Walleska De Jesús-Bonilla[¶], Juan López-Garriga[¶][1], Ariel Lewis[¶], Ruth Pietri[¶], Syun-Ru Yeh[‖], Carmen L. Cadilla[**], and Juan Manuel García-Ruiz[‡]

From the [‡]Laboratorio de Estudios Cristalográficos, CSIC, P.T. Ciencias de la Salud, 18100, Granada, Spain, the [§]Department of Química-Física, Bioquímica y Química Inorgánica, Universidad de Almería, Carretera Sacramento, Almería, 04120, Spain, [¶]Chemistry Department, P. O. Box 9019, University of Puerto Rico, Mayagüez Campus, Mayagüez 00681, Puerto Rico, the [‖]Department of Physiology and Biophysics, Albert Einstein College of Medicine, Bronx, New York 10461, and the [**]Biochemistry Department, Medical Sciences Campus, University of Puerto Rico, San Juan, Puerto Rico 00936

Lucina pectinata ctenidia harbor three heme proteins: sulfide-reactive hemoglobin I (HbI_{Lp}) and the oxygen transporting hemoglobins II and III ($HbII_{Lp}$ and $HbIII_{Lp}$) that remain unaffected by the presence of H_2S. The mechanisms used by these three proteins for their function, including ligand control, remain unknown. The crystal structure of oxygen-bound $HbII_{Lp}$ shows a dimeric oxy$HbII_{Lp}$ where oxygen is tightly anchored to the heme through hydrogen bonds with Tyr^{30}(B10) and Gln^{65}(E7). The heme group is buried farther within $HbII_{Lp}$ than in HbI_{Lp}. The proximal His^{97}(F8) is hydrogen bonded to a water molecule, which interacts electrostatically with a propionate group, resulting in a Fe-His vibration at 211 cm^{-1}. The combined effects of the $HbII_{Lp}$ small heme pocket, the hydrogen bonding network, the His^{97} trans-effect, and the orientation of the oxygen molecule confer stability to the oxy-$HbII_{Lp}$ complex. Oxidation of HbI_{Lp} Phe(B10) → Tyr and $HbII_{Lp}$ only occurs when the pH is decreased from pH 7.5 to 5.0. Structural and resonance Raman spectroscopy studies suggest that $HbII_{Lp}$ oxygen binding and transport to the host bacteria may be regulated by the dynamic displacements of the Gln^{65}(E7) and Tyr^{30}(B10) pair toward the heme to protect it from changes in the heme oxidation state from Fe^{II} to Fe^{III}.

Hemoglobins are key proteins in symbiotic relationships between invertebrates and chemoautotrophic bacteria. The clam *Lucina pectinata* inhabits the sulfide-rich tropical mud and produces three different types of hemoglobin in its gills, first described by Read (1) and characterized by Kraus and Wittenberg (2, 3). Different functionalities have been described for the three hemoglobin variants: hemoglobin I (HbI_{Lp})[2] is a sulfide-reactive monomeric protein, whereas hemoglobin II and III ($HbII_{Lp}$ and $HbIII_{Lp}$) are oxygen transporters. $HbII_{Lp}$ and $HbIII_{Lp}$ self-associate in a concentration-dependent manner forming a tetramer that remains unaffected in the presence of H_2S (2, 3). The mechanisms underlying ligand selection control between HbI_{Lp} and $HbII_{Lp}$/$HbIII_{Lp}$ remain unknown. The structure of HbI_{Lp} has been solved with different ligands bound at the distal position: water (Protein Data Bank code 1FLP) (4), cyanide (PDB code 1BOB) (5), and hydrosulfuric acid (PDB code 1MOH) (6). The primary structure of $HbII_{Lp}$ was determined by Edman degradation (7) and from its cDNA sequence (8). HbI_{Lp} only shares 32% of its amino acid sequence with $HbII_{Lp}$, but both have a conserved glutamine in the E7 position, and a phenylalanine and a tyrosine in the B10 position for HbI_{Lp} and $HbII_{Lp}$, respectively. The Tyr(B10) and Gln(E7) distal heme pocket residues of $HbII_{Lp}$ are also found in other hemoglobins (8, 9). Hemoglobins from *Ascaris suum* (Hb_{Asc}) (Tyr(B10) and Gln(E7)) (10) and *Mycobacterium tuberculosis* hemoglobin N (Tyr(B10) and Leu(E7)) (11, 12) show high oxygen affinity and a very slow release of the bound oxygen. The three different hemoglobins from the clam *Scapharca inaequivalvis* (Hb_{Si}) show a very different heme pocket (Met(B10) and His(E7)) (13). $Hb_{IIA, Si}$ and $Hb_{IIB, Si}$, assemble to form a heterotetramer (like $HbII_{Lp}$ and $HbIII_{Lp}$), whereas $Hb_{I, Si}$ forms homodimers (like $HbII_{Lp}$). The different types of hemoglobin from this clam bind oxygen cooperatively. $Hb_{IIB, Si}$ exhibits a Hill coefficient for oxygen binding of 2.1 when in a heterotetramer, whereas the homodimer has a Hill coefficient of 1.5 (14). Interestingly, even though the *S. inaequivalvis* hemoglobins and *L. pectinata* $HbII_{Lp}$ and $HbIII_{Lp}$ share ≥40% amino acid similarity, the *Lucina* hemoglobins do not behave cooperatively (2).

[2] The abbreviations used are: Hb_{Lp}, *L. pectinata* hemoglobin; Hb_{Asc}, *A. suum* hemoglobin; Hb_{Si}, *S. inaequivalvis* hemoglobin; HbIr, *L. pectinata* recombinant HbI; trHb, truncated hemoglobins; FPLC, fast performance liquid chromatography; BisTris, 2-[bis(2-hydroxyethyl)amino]-2-(hydroxymethyl)propane-1,3-diol.

Early biophysical studies (15) compared the structure and functionality of $HbII_{Lp}$ and hemoglobin from *A. suum* because both heme proteins have heme pockets with Tyr(B10) and Gln(E7). The low oxygen off rates were attributed to differences in the hydrogen bonding network of both oxy-protein complexes. Additional studies using UV-visible spectroscopy and pH titration of $HbII_{Lp}$ and a HbI_{Lp} Phe(B10) → Tyr mutant have revealed bands at 486, 541, 577, and 603 nm for both proteins at neutral conditions (3, 9). At basic pH values, the barrier for the reaction increases as the tyrosine adopts a closed conformation and the heme (Fe^{III}) hydroxyl complex replaces the met-aquo species, which suggested the existence of an open and closed conformation due to the interactions between Tyr(B10) and the heme iron. The presence of these conformers were confirmed by resonance Raman spectroscopy showing that, in a neutral environment, met-aquo $HbII_{Lp}$ was present as a mixture of coordination and spin states with values for the ν_2 mode at 1558 cm^{-1} (6C HS) and 1580 cm^{-1} (6C LS) and for the ν_3 mode at 1479 cm^{-1} (6C HS), 1492 cm^{-1} (5C), and 1503 cm^{-1} (6C LS) (9). The infrared spectra of the complex $HbII_{Lp}CO$ also showed the presence of the A_3 (closed) and A_0 (open) conformers at 1924 and 1964 cm^{-1}, respectively (9). We proposed that in the open conformation Tyr(B10) swings away from the heme iron, whereas in the closed conformation Tyr(B10) is closer to and may interact with the ligand. Similarly, the reactions between hydrogen peroxide and both $HbII_{Lp}$ and the HbI_{Lp} Phe(B10) → Tyr mutant showed that Tyr(B10) tailors, in two very distinct ways, the reactivity of compounds I and II ferryl species (9). First, increasing the reaction pH from 4.9 to 7.5, and then to 11.2, the second order rate constant for $HbII_{Lp}$ decreases from 141.60 to 77.78 $M^{-1} s^{-1}$, and to 2.96 $M^{-1} s^{-1}$, respectively. This pH dependence is associated with the disruption of the heme-tyrosine (603 nm) protein moiety, which controls access of H_2O_2 to the heme protein active center, thus regulating the formation of the ferryl species. Second, the existence of a hydrogen bonding network between the heme pocket amino acids (*i.e.* Tyr(B10)) and ferryl compound I created a much faster path than $3.0 \times 10^{-2} s^{-1}$ for the decay of compound I to compound II. Moreover, the presence of Tyr(B10) in $HbII_{Lp}$ and the HbI_{Lp}Phe(B10) → Tyr mutant appears to afford a more stable O_2 adduct in the oxygenated HbI_{Lp}. The contribution of Tyr(B10) to the stability of the $HbII_{Lp}$ and HbI_{Lp} Phe(B10) → Tyr heme pocket against peroxide attack has recently been shown to be partially due to the presence of hydrogen bonding between the ferryl moiety and the heme pocket amino acids, including Tyr(B10), which ultimately enhances the removal of peroxide by the peroxidative cycle (16, 17). In addition, the close proximity of Tyr(B10) with Gln(E7) to the heme iron contributes largely to the distal control of NO binding, thus providing a model for the design of future oxidative stable oxygen hemoglobins with little or no vasoactivity (16).

Here, we report detailed structural data of $HbII_{Lp}$ obtained by x-ray crystallography, providing information about the heme pocket, distal amino acids, and their interaction with the dioxygen molecule. Our results, supported by resonance Raman measurements, suggest a mechanism where $HbII_{Lp}$ selects oxygen by tailoring the hydrogen bonding environment between the Tyr(B10) and Gln(E7) and heme-O_2 moiety, stabilizing the heme (Fe^{II}) oxidation state.

EXPERIMENTAL PROCEDURES

Wild-type HbI_{Lp} and $HbII_{Lp}$ Sample Preparations—Proteins were isolated and purified as described with minor modifications (9). HbI_{Lp} was separated from $HbII_{Lp}/HbIII_{Lp}$ using a Hi Load 26/60 Superdex 200 gel filtration column (AKTA FPLC, Amersham Biosciences). HbI_{Lp} was further purified by cation exchange chromatography using DEAE Sephadex Fast Flow equilibrated with 25 mM ammonium bicarbonate buffer, pH 8.3. $HbII_{Lp}$ was purified from the $HbII_{Lp}/HbIII_{Lp}$ fraction by ion exchange chromatography with a HiPrep 16/10 Q FF column equilibrated with 10 mM triethanolamine/acetate buffer at pH 8.3 and eluted with a gradient of sodium chloride concentration from 0 to 180 mM. The purity of the proteins was confirmed by SDS-PAGE.

Recombinant HbI_{Lp} and Site-directed Mutant Preparation— The mutants from *L. pectinata* HbI (HbI_{Lp}Phe(B10) → Tyr, HbI_{Lp}Gln(E7)Val, HbI_{Lp}Gln(E7) → Asn, and HbI_{Lp}Gln(E7) → His) were obtained by introducing single amino acid substitution using the QuikChange Mutagenesis kit (Stratagene, La Jolla) into the HbI_{Lp} coding region cloned into the pET28(a+) vector (18). The HbI_{Lp} mutants were expressed in *Escherichia-coli* Bli5 cells as described (18). Dark red cell pellets were lysed and centrifuged to separate the soluble from the insoluble fractions. The soluble fraction was equilibrated with CO and purified in Co^{2+} affinity columns (Talon, Invitrogen) followed by size exclusion chromatography (AKTA FPLC, Amersham Biosciences) (9). The purified HbI_{Lp}Phe(B10) → Tyr showed UV-visible spectra typical of an oxy$HbII_{Lp}$. Met-aquo and CO HbI_{Lp}Phe(B10) → Tyr derivatives were obtained in a similar manner as the $HbII_{Lp}$ complexes (18).

$HbII_{Lp}$ Sequence Analysis—Amino acid sequences were obtained from the NCBI protein sequence data base. The accession numbers for *L. pectinata* hemoglobins are HbI AAG01380, HbII AAO89499, and HbIII AAB28352. Data base searches for sequences with high sequence similarity was performed using the $HbII_{Lp}$ sequence and PSI-BLAST (19). Multiple sequence alignments were performed with ClustalW (20). Sequence alignments were used to assess the variation at specific positions and the resulting differences in the overall structure and distal heme cavity.

Crystallization and Data Collection—$HbII_{Lp}$ was crystallized as previously reported (21). In brief, lyophilized $HbII_{Lp}$ was dissolved in 50 mM BisTris propane pH 7.0 buffer, 0.5 mM EDTA in a final concentration of 30 mg/ml. The crystals were grown by the counter-diffusion technique with a three-chamber configuration (22) using ammonium sulfate as precipitant. X-ray diffraction intensity data were collected at the BM-16 station of the European Synchrotron Radiation Facility (ESRF) using a 0.97-Å wavelength in a Mar CCD-165 detector. Data were indexed, integrated, and scaled with HKL2000 suite (23) at a resolution limit of 1.93 Å.

Structure Solution and Refinement—The structure of $HbII_{Lp}$ was solved by molecular replacement methods as reported in Ref. 21. In brief, coordinates from HbI_{Lp} (PDB code 1EBT) without the water molecule present in the distal position of the

TABLE 1

Data collection and refinement statistics of HbII$_{LP}$-O$_2$ structure

Statistical values for the highest resolution shell, 1.96–1.93 Å for data collection and 1.98–1.93 Å for refinement, are given in parentheses.

Data collection	
Wavelength (Å)	0.977
Temperature (K)	100
Space group	P4$_2$2$_1$2
$a = b, c$ (Å)	73.92, 152.35
α, β, γ (°)	90
Monomers per asymmetric unit	2
Resolution (Å)	20.0-1.93
No. of observed reflections	338,327
Redundancy	10.5 (10.6)
Completeness (%)	99.6 (100.0)
R_{merge}[a] (%)	5.0 (33.6)
Average $I/\sigma(II)$	40.0 (7.0)
Refinement	
R value (%)	16.5 (17.5)
R_{free} value (%)	19.3 (22.5)
No. of reflections in working set	30,675 (2158)
No. of reflections in test set	1,643 (137)
No. of solvent molecules	283
Average B factor (Å2)	30.42
Root mean square deviations bond length (Å)	0.013
Root mean square deviations bond angles (°)	1.841
Ramachandran plot	
Most favored regions (%)	94.8
Allowed regions (%)	5.2
General allowed regions (%)	0.0
Disallowed regions (%)	0.0

[a] $R_{\mathrm{merge}} = \Sigma_{hkl}\Sigma_i |\langle I \rangle - I_i|/\Sigma_{hkl}\Sigma_i (I_i)$.

FIGURE 1. **Structure of the HbII dimer from *L. pectinata*.** Each helix, A to H, is labeled and identified by the colors: *red*, *blue*, *yellow*, *magenta*, *orange*, *pink*, *light blue*, and *salmon*, respectively.

heme iron were used as a search model and the molecular replacement solution was found using the CNS suite (24). Refinement was conducted using CNS and REFMAC5 software from CCP4 (25). After several cycles of restrained refinement, manual model building against the electron density maps was conducted with the program COOT (26). Once all the residues were replaced by the HbII$_{LP}$ sequence, the R-factor and R-free decreased to 0.30 and 0.36, respectively. Additional refinement was carried out with REFMAC5 using the TLS parameters (27). The inclusion of TLS parameters in the refinement process improved the R-factor and R-free to a final value of 0.17 and 0.19, respectively. Water molecules were placed in electron density difference maps using the ARP/wARP version 5.0 program from the CCP4 suite. All the structures were checked using the refinement with MolProbity (28), and before deposition using PROCHECK (29). Details on data collection and structure refinement are summarized in Table 1. The secondary structure was tested with iMolTalk (30), whereas β-turn geometry was calculated using the program PROMOTIF version 2.0 (31). Superposition and root mean square deviations of the structures were performed using the CCP4 program LSQKAB (32). Protein interfaces in the crystal were characterized using the PISA server (33). Distances between amino acids were calculated using the program CONTACT from CCP4 (25). The accessible surface areas values were computed with NACCESS (34) with a probe radius of 1.4 Å and a slice width of 0.05 Å. Protein cavities were computed using the CASTp server (35). The coordinates and structure factors of *L. pectinata* HbII were deposited at the RCSB PDB with entry code 2OLP.

Potassium Ferricyanide Titration and Resonance Raman Spectroscopy—Deoxyhemoglobin was obtained by adding sodium dithionite to the purified protein samples, followed by a purification step in a Hi-Trap desalting column (FPLC, GE Healthcare). Oxyhemoglobin complexes were obtained by flushing the deoxy derivatives with oxygen. The initial concentration for the oxyHb$_{LP}$ species was 3.40 μM, at pH 7.5. The titration of oxyHbI$_{LP}$ was initiated with the addition of 15-μl aliquots of a 10% potassium ferricyanide solution (2) up to a total volume of 150 μl to obtain the met-aquo HbI$_{LP}$. Full oxidation of HbII$_{LP}$ and the HbI$_{LP}$Phe(B10) → Tyr mutant proteins required a decrease of pH from 7.5 to 5.0, because the above conditions were not adequate. The resonance Raman measurements were made by focusing the output of a krypton ion laser at 413.1 nm (Spectra Physics) to a ~30-μm spot on a rotating cell to prevent photodamaging. The laser power was set at 10 milliwatts using a CCD back-illuminated detector (800 × 2000 pixels) coupled to a modified Spex 1401 centered at 410 nm. Three spectra were collected, each composed of 60 accumulations of 10 s. Hemoglobin concentration was ~100 μM.
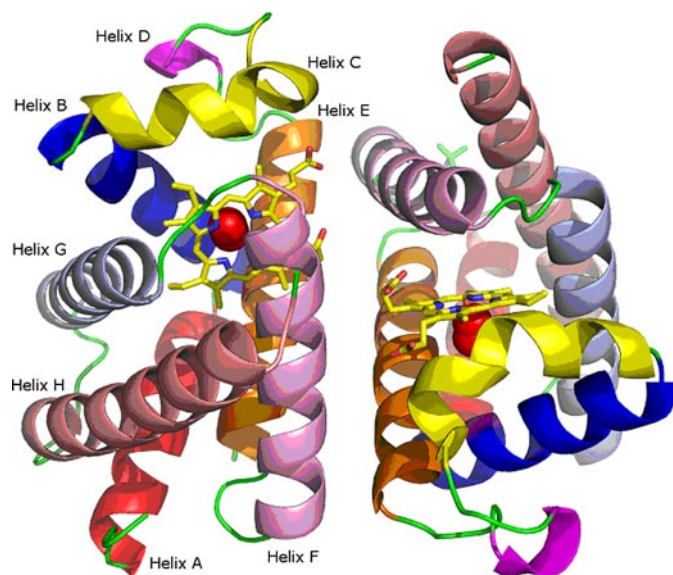
RESULTS

HbII$_{Lp}$ Structure and Sequence Analysis—The HbII$_{LP}$ crystallizes in space group P4$_2$2$_1$2, and diffracts x-rays with a resolution better than 2.0 Å, having unit cell parameters $a = b = $ 73.92 Å and $c = 152.35$ Å, and two molecules forming a dimer in the asymmetric unit and a solvent content of 61% per volume. All the residues are placed in the most favorable region of the Ramachandran plot. HbII$_{LP}$ shows the characteristic globin fold with six α-helices surrounding the central heme pocket, and two minor helical segments between B and E helices (Fig. 1). The distance between the iron atoms in the dimer is 17.8 Å, and the plane orientation of the porphyrin ring is almost perpendicular. This short distance between the heme groups is a characteristic feature of the EF-dimers in other types of molluscan hemoglobin (36). The dimer interface includes 25 residues of each monomer and covers a surface of 845 Å^2. At the interface, four hydrogen bonds, namely, Lys[95B]–Ser[46A] (2.77 Å),

FIGURE 2. **Multiple sequence alignment of the three types of hemoglobin from *L. pectinata*, the bivalve mollusk *S. inaequivalvis*, and domain one of the nematode *A. suum* hemoglobin.** The corresponding helices as predicted by the program suite iMoltalk applying the STRIDE method are labeled (*red squares*). Conserved residues are shaded in *cyan* and residues at position B10 (Tyr[30] in *L. pectinata*), E7 (Gln[65] in *L. pectinata*), Lys[92] and Arg[100] (*L. pectinata*) are shaded in *yellow*. The gaps are labeled in *green*.
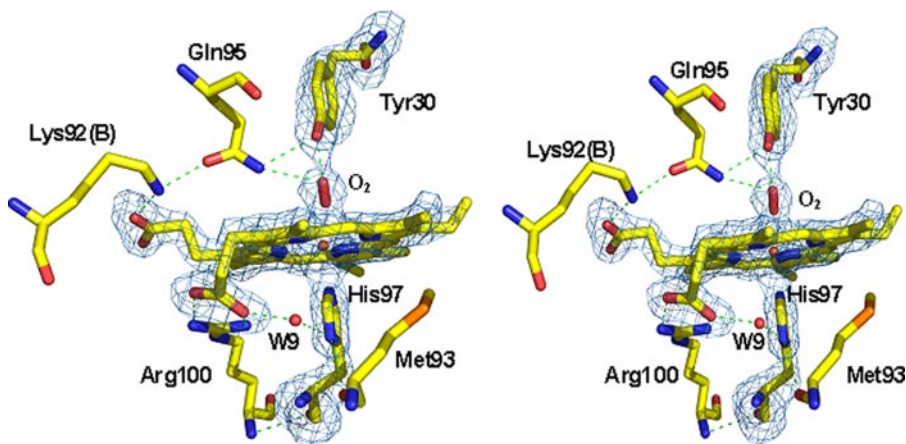
FIGURE 3. **Stereo view of the hydrogen bond network in the oxygen bound HbII$_{LP}$ structure.** Residues at a 5-Å distance cut-off are shown. The omit map (contoured at 3 σ) and bond interactions are shown in *blue* and *green lines*, respectively. Distances between residues are shown in Table 2.

Lys[95A]–Ser[46B] (2.98 Å), Lys[92B]–Gln[65A] (2.73 Å), and Lys[92A]–Gln[65B] (2.66 Å), and one salt bridge Asp[82B]–Lys[63A] (3.05 Å) are found. It is noteworthy that the HbII$_{LP}$ structure confirms the existence of one aspartate in position 84 and an acetyl group in the N terminus as previously suggested by comparison of matrix-assisted laser desorption ionization-mass spectrometry results and the cDNA-derived amino acid sequences (8).

The sequence alignments of the hemoglobins of *L. pectinata, S. inaequivalvis,* and *A. suum* are shown in Fig. 2. The multiple alignment has three gaps: one between the C and D helices, a second one within the G helix, and the third gap after the G helix. The B10 residue varies from a Phe in HbI$_{LP}$, Tyr in HbII$_{LP}$, HbIII$_{LP}$, and Hb$_{Asc}$ to a Met in the three types of hemoglobins from *S. inaequivalvis*, whereas the E7 position contains a His

residue in all the *S. inaequivalvis* hemoglobins and a Gln in the rest of the aligned polypeptides. In the HbII$_{LP}$ structure, the Arg[100](F11) and Lys[92](F3) form H-bonds with the propionates of the heme group. The Lys[92](F3) and Arg[100](F11) are conserved in all the hemoglobin sequences, except in Hb$_{Asc}$ that are replaced by Glu[92] and Asp[100], respectively. The replacement of Lys[92] by a Phe[93] in the HbI$_{LP}$, which cannot form the salt bridge or hydrogen bonds, suggests that Lys[92] could be responsible for the HbII$_{LP}$ dimer stability.

HbII$_{LP}$ is known to form large aggregates at high concentrations (2). Analysis for protein complex assembly using the PISA Server (31) predicted two additional assemblies: a dimer of dimers to form a tetramer, and a dimer of the tetramer to form an octamer, both of low predicted stability. The superposition of the HbII$_{LP}$ dimer with Hb$_{I,Si}$ has an overall average root mean square deviation of 2.2 Å (supplemental Fig. 1). The tetrameric Hb$_{IIAB,Si}$ in the form of two heterodimers is composed by chains Hb$_{IIA,Si}$ and Hb$_{IIB,Si}$ (37). The hypothetical HbII$_{LP}$ tetramer in the unit cell is different from that of the *S. inaequivalvis* hemoglobin.

A channel of water molecules is buried in the HbII$_{LP}$ dimer interface, 40 of them located at a distance <10 Å of the heme groups. They form H-bonds with several residues located between the heme groups in the dimer. This interfacial water has been previously reported in the homodimeric Hb$_{I,Si}$ contained in the coelomic fluid erythrocytes from the bivalve mollusk *S. inaequivalvis* (38) and they have been proposed to play an important role in the allosteric behavior of hemoglobin Hb$_{I,Si}$ (39).

The major differences between chains A and B in the *L. pectinata* HbII dimer are found in the β-turn formed by residues Gly[122]-Gly[123]-Leu[124]-Thr[125] with a maximum root mean square deviation of 3.4 Å. The β-turn is a type I in chain A, and a type IV in chain B. This difference in conformation arises from a difference in the environment, the β-turn has several contacts with the symmetry related molecule in chain A, whereas in chain B, it is exposed to the solvent. This β-turn is also one of the major differences between the HbII$_{LP}$ and HbI$_{LP}$ structures.

TABLE 2
Heme contacts in HbII$_{Lp}$-O$_2$ structure

Residue 1	Atom	Residue 2	Atom	Distance (Å)	
				Chain A	Chain B
HEM	O1A	Arg[100]	NH$_2$	2.71	2.52
		W6/W7	O	2.62	2.57
	O2A	Arg[100]	NH1	2.98	2.88
		Arg[100]	NH$_2$	3.47	3.34
		W9/W2	O	2.59	2.63
	O1D	Lys[92][a]	NZ	2.63	2.72
		W43/W5	O	2.64	2.67
	O2D	W8/W3	O	2.62	2.66
		W34/W5	O	2.59	3.41
		W43/33	O	3.42	2.62
		W57/139	O	2.96	2.98
	Fe	His[97]	NE2	2.08	2.04
		Oxy	O1	2.94	2.85
		Oxy	O2	2.11	1.69
Tyr[30]	OH	Gln[65]	NE2	3.00	3.07
		Oxy	O1	1.94	1.78
		Oxy	O2	2.99	2.95
His[97]	ND1	Met[93]	O	2.98	2.79
		W9/W2	O	3.45	3.41
Q65A	OE1	Lys92[a]	NZ	2.73	2.66
	NE2	Tyr[30]	OH	3.00	3.07
		Oxy	O1	3.02	3.04
		Oxy	O2	3.43	3.51

[a] Marked contacts are inter-polypeptides chains.

FIGURE 4. **Resonance Raman spectra of deoxy samples of (a) HbI$_{Lp}$, (b) HbI$_{Lp}$Phe(B10) → Tyr, and (c) HbII$_{Lp}$ showing the Fe-His stretching mode and trans-effect of the proximal His.**

HbII$_{Lp}$ Distal and Proximal Heme Pocket—Fig. 3 shows the structure and the hydrogen bonding network of the oxyHbII$_{Lp}$ proximal and distal sites. The porphyrin ring adopts a planar configuration with the iron atom in the plane, and the average distance of the pyrrolic nitrogens to the iron is 2.06 Å. The dioxygen forms an angle of 123° with the iron atom in chain A, and 162° in chain B. The heme pocket in chain B is slightly smaller than in chain A and the distance between the OH of the distal tyrosine and the iron atom is shorter (4.84 Å in chain A and 4.53 Å in chain B, but the differences in the volume size of the heme cavity are 912.6 Å^3 in chain A and 831.9 Å^3 in chain B) might arise from small differences in the position of the atoms as a consequence of the average coordinates position. In the HbII$_{Lp}$ heme cavity most of the aromatic residues are conserved when compared with HbI$_{Lp}$ (for instance, Trp(A11), Phe(B9), Phe(C7), Phe(CD5), Phe(E11), and Trp(H8)), except Tyr(B10), Tyr(G8), and Tyr(G14), which are replaced by phenylalanine in the HbI$_{Lp}$ sequence, and Phe(E18) that is replaced by tryptophan. Although the HbII$_{Lp}$ proximal heme pocket is mainly hydrophobic, it contains one buried water molecule (W^9). This water molecule forms a hydrogen bond with the heme propionate group (O2A) within a distance of 2.59 Å and with His[97](ND1) within a distance of 3.45 Å (Table 2). It is also part of the water network in the interface of the HbII$_{Lp}$ dimer. A water molecule is also present in the heme pocket of the HbI$_{Lp}$ as part of an identical hydrogen network.

When HbI$_{Lp}$ and HbII$_{Lp}$ are superimposed using the heme group as a reference, the HbI$_{Lp}$ as well as the proximal histidine show a displacement of ~1 Å. The orientation of the proximal His[97](F15) is roughly perpendicular to the heme plane and the average distance between the His[97](NE2) atom and the iron atom is 2.06 Å, which is a slightly shorter distance when compared with the sulfide (PDB code 1MOH), cyanide (PDB codes 1ETB and 1B0B), and water-bound HbI$_{Lp}$, where the distances range from 2.13 to 2.31 Å. It has been suggested that within the various kinds of hemoglobin and myoglobin a hydrogen bond
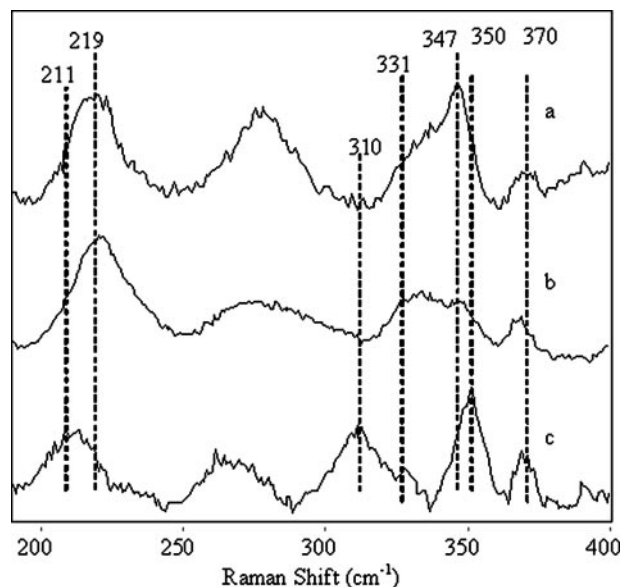
between the proximal histidine His(F8) and the side chain of a residue next to it modulates the strength of the His-Fe bond, regulating the ligand affinity (37, 40). In HbII$_{Lp}$, His(F8) has two possible hydrogen bond interactions, the first one with the buried water molecule and the second one from the interaction of the carbonyl group of Met[93] and the ND1 from histidine (Table 2). A similar hydrogen bond is formed between the carbonyl of Met[93] and the histidine ND1 atom in HbI$_{Lp}$.

Heme Oxidation and Resonance Raman Spectra of Oxy Species—HbI titration with potassium ferricyanide required an additional oxidizing agent to complete oxidation to the met-aquo HbI$_{Lp}$ form, shifting the Söret band from 416 nm (oxyHbI$_{Lp}$) to a maximum at 407 nm (supplemental Fig. 2). A pH-dependent titration for oxyHbII$_{Lp}$ and the oxyHbI$_{Lp}$-Phe(B10) → Tyr mutant required a decrease in pH from 7.5 to 5.5 to completely change the Söret band from 414 to 403 nm, a characteristic of the met-aquo HbII$_{Lp}$ species. This result suggests that Tyr in the B10 position is responsible for the pH oxidation control of oxyHbII$_{Lp}$ and the oxyHbI$_{Lp}$Phe(B10) → Tyr mutant. Similarly, Fig. 4 compares the low frequency resonance Raman spectra of ferrous deoxygenated recombinant HbI$_{Lp}$, HbI$_{Lp}$Phe(B10) → Tyr, and HbII$_{Lp}$, which provides information on the Fe-His stretching mode (ν_{FeN}) and the trans-effect of the proximal histidine on the Fe-O$_2$ mode. The vibrational frequencies (Fig. 4, *a* and *b*) for HbI$_{Lp}$ and the HbI$_{Lp}$Phe(B10) → Tyr mutant are located at 219 cm^{-1}, similar to the myoglobin spectrum. However, for HbII$_{Lp}$ the ν_{FeN} is present at a lower frequency, 211 cm^{-1} (Fig. 4*c*), suggesting that the factors controlling the strength of the Fe-N bond are not the same for both sets of hemoproteins. Normal mode assignments were based on the presence or absence of a particular frequency on the spectra for the HbI$_{Lp}$-ligand complexes and compared with the values reported in the literature (17, 41). The ν_{FeN} for hemoglobin and myoglobin has been found in the resonance Raman spectra between the 217 and 244 cm^{-1} regions (17, 41, 42). The spectra also show a band at 370 cm^{-1}, which has pre-
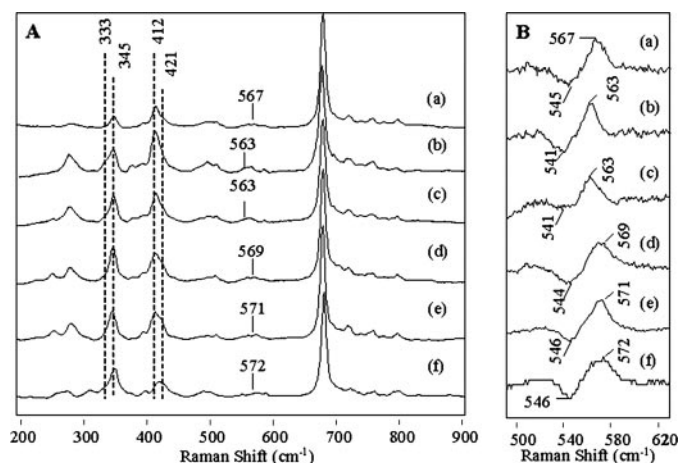
FIGURE 5. *A*, resonance Raman spectra of oxy species HbII$_{LP}$, HbI$_{LP}$, and HbI$_{LP}$ mutants. *B*, oxygen isotopic shift for the Fe-O$_2$ normal mode vibration of the oxyHbII$_{LP}$, oxyHbI$_{LP}$, and oxyHbI$_{LP}$ mutants.

viously been attributed to the C$_\beta$-C$_c$-C$_d$ bending motion of the peripheral propionate heme substituents in HbI$_{LP}$. The spectra for HbI$_{LP}$ and HbI$_{LP}$Phe(B10) → Tyr also show the ν_8 band at 347 cm^{-1}. This is characteristic of the combination of the metal-pyrrole stretch and the in-plane substituent bend, and a shoulder at 331 cm^{-1} that has been assigned to the out-of-plane pyrrole-tilting mode. In contrast, in HbII$_{LP}$ the spectral bands have been displaced to 350 and 310 cm^{-1}, respectively.

Fig. 5*A* shows the vinyl region and the Fe-O$_2$ vibration for HbII$_{LP}$, recombinant HbI$_{LP}$ and a series of HbI$_{LP}$ mutants. Some differences in their vibrational modes are observed as function of the polarity of the heme pocket and oxygen isotopic substitution. For example, the recombinant HbI$_{LP}$ (Fig. 5*A*, *a*) shows a relatively strong band at 412 cm^{-1} with a small shoulder at 421 cm^{-1}. The former corresponds to an in-plane vinyl-bending mode (δC$_b$C$_\alpha$C$_\beta$-vinyl), whereas the latter is attributed to either a contribution from both vinyls or the same vinyl reflecting heterogeneity among heme subunits. Only small intensity changes are observed as a function of amino acid substitution. Similarly, the ν_8 band is found at 345 cm^{-1}, which is invariant among the different hemeprotein derivatives. The shoulder of the out-of-plane pyrrole-tilting mode at 333 cm^{-1} is almost absent in the samples. Fig. 5*B* shows the ^{16}O$_2$–^{18}O$_2$ isotope difference spectra, where the Fe-O$_2$ stretching mode of the heme O$_2$ moiety presents a significant frequency change as a function of the heme pocket amino acids. Thus, the spectrum of recombinant HbI$_{LP}$ (Fig. 5*B*, *a*) shows a band at 567 cm^{-1}, which was previously attributed to the Fe-O$_2$ stretching mode, and in this work, has been confirmed by the oxygen isotopic substitution. Changing the residue at the E7 position in the HbI$_{LP}$Gln(E7) → Val and HbI$_{LP}$Gln(E7) → Asn mutants (Fig. 5*B*, *b* and *c*) produced a decrease in the stretching mode to 563 cm^{-1}, whereas changing the residue at the E7 position with the HbI$_{LP}$Gln(E7) → His or at the B10 position in HbI$_{LP}$Phe(B10) → Tyr mutants (Fig. 5*B*, *d* and *e*) increased the frequency of the Fe-O normal mode to 569 and 572 cm^{-1}, respectively. For the wild-type HbII$_{LP}$ this frequency is present at 573 cm^{-1} (Fig. 5*B*, *f*), suggesting that the oxygen in the heme O$_2$ moiety is strongly hydrogen bonded to the

distal pocket Tyr^{30}(B10) and Gln^{65}(E7), in good agreement with the proposed x-ray structure.

DISCUSSION

The crystal structure of oxyHbII from *L. pectinata* has been solved and it shows relevant differences when compared with the ferric HbI$_{LP}$ sequence and structure (the oxyHbI$_{LP}$ structure has not been resolved yet). The overall hemoglobin fold is conserved in these clam proteins. Some important differences between them are found in the additional residues in the sequence of HbII$_{LP}$ and the flexible β-turn formed by the GGLT residues. The heme cavity is conserved between the HbI$_{LP}$ and HbII$_{LP}$ forms, with the exception of the B10 position, which is occupied by Phe and Tyr, respectively. A significant displacement of the heme group is observed in the least square superimposition of both types of hemoglobins. The heme group is buried farther in HbII$_{LP}$ than in HbI$_{LP}$ because of the minor steric hindrance of the Met^{93} and Phe^{76} residues that are replaced by Phe^{92} and Trp^{75}, respectively. Oxygen is tightly bound to the HbII$_{LP}$ heme distal site through simultaneous hydrogen bonds with Tyr(B10) and Gln(E7) (Fig. 3). This last pair of amino acids has been proposed to stabilize the oxygenated form of HbII$_{LP}$ by means of strong and weak hydrogen bonds, respectively (37, 40). Hb$_{Asc}$ also has a Tyr(B10) and a Gln(E7), and a high oxygen affinity and unusually slow off rate for oxygen dissociation (15, 41). The Hb$_{Asc}$ crystal structure (PDB 1ASH) shows that the distance between the iron to oxygen O1 is 1.90 Å, and between Tyr(B10)(OH) to O$_2$ is 2.73 Å (40). Table 2 presents several distances between the oxygen heme moiety and the amino acids in the distal pocket of HbII$_{LP}$. For example, the iron to oxygen O1 is 2.94 Å, and from Tyr(B10)(OH) to O$_2$ is 2.99 Å. These longer distances are rather similar to those found in the structure of *M. tuberculosis* hemoglobin N (12). The orientation of the dioxygen bound to the heme plane is 110°, similar to the value found in the HbII$_{LP}$ structure, but in this case, the oxygen molecule is pointing toward the Tyr(B10)(OH) group. A CASTp calculation resulted in an average volume of 1000 Å^3 for the heme cavity in *M. tuberculosis* hemoglobin, which is slightly larger than the average size of 872 Å^3 for HbII$_{LP}$. Similarly, a large cavity volume was observed in the ferric derivative of the Mb triple mutant (L29F/H64Q/V68F), Mb, and HbI$_{LP}$. The crystal structure reveals the existence of a much greater heme freedom and larger distal cavity volume in HbI$_{LP}$ than sperm whale Mb, in both the H$_2$S bound and unbound to the heme group, because of the lack of hydrogen bonding between the heme propionate groups and nearby amino acid residues (43). This dynamic behavior is absent in HbII$_{LP}$, where the heme group is firmly anchored in place.

Cooperativity and Allosteric Effects—In contrast to a remarkably conserved tetrameric arrangement in vertebrate hemoglobins, invertebrate hemoglobins show a large diversity in quaternary structures (36). The aggregation state of the hemoglobin plays a central role in their cooperative behavior. Hemoglobins from *L. pectinata* show that HbI$_{LP}$ is a monomer in all of the conditions assayed, whereas HbII$_{LP}$ and HbIII$_{LP}$ behave as apparent monomers at low concentrations and aggregates at higher concentrations (2). Lys^{92} of HbII$_{LP}$ may play an impor-

tant role in dimer stability, because a Thr that disrupts the possibility to form a bond between chains replaces this residue in the HbI$_{LP}$ sequence. Lys[92] is conserved in HbIII$_{LP}$ opening up the possibility to form a heterodimer as occurs in *S. inaequivalvis* hemoglobins. The oligomeric hemoglobins from *S. inaequivalvis* show cooperativity in oxygen binding. However, a Hill coefficient of 1.1 was obtained for the oxygen binding measurement of HbII$_{LP}$, regardless of the aggregation state (2, 3). Several mutant forms of the Hb$_{I, Si}$ dimer have structurally characterized, suggesting that two residues play an important allosteric role. First, Phe[97](F3) is packed tightly in the heme pocket in the deoxy Hb$_{I, Si}$ state, and exposed to the dimer interface upon ligand binding (44). The displacement of the bulky Phe[97] side chain to the dimer interface displaces several water molecules leaving the interface with less water and a poorer ordered water network. A similar behavior has been described for the heterotetramer of Hb$_{IIA, Si}$ and Hb$_{IIB, Si}$ in which mutation of the Phe[97] to leucine provokes a loss of cooperativity (44). Another residue playing a determinant role is Thr[72], and both Phe[97] and Thr[72] are replaced in HbII$_{LP}$ by methionine and valine, respectively.

The superpositions of the HbII$_{LP}$ structure to the oxygen bound (PDB code 3SDH) and unbound (PDB code 4SDH) hemoglobin states of the *S. inaequivalvis* show that Asn[100] in these hemoglobins is replaced by Leu[96] in HbII$_{LP}$, leading to the loss of a strong hydrogen bond between Asn[100] and the heme propionate group. Moreover this propionate moiety of the heme group in *S. inaequivalvis* shows an important displacement between the oxygen-bound and unbound forms. In particular, the orientation of the unbound form is equivalent to the orientation of the propionate in the oxyHbII$_{LP}$ structure. The interaction with the nearest residues is the same in Hb$_{Si}$, even a water molecule equivalent to the water molecule (W[9]) bound to His[97] (Fig. 3) is found at a distance of 2.52 Å. Interestingly, this water molecule disappears in the oxygen-bound structure of *S. inaequivalvis*. This observation supports the hypothesis that this water molecule plays an important role in the regulation of the heme group affinity to ligands.

Geometry of the Heme-Oxygen Moiety and Hydrogen Bonding Network—The hydrogen bonding network between the heme bound oxygen and the Gln(E7) and Tyr(B10) of HbII$_{LP}$ is almost identical to the active center of Hb$_{Asc}$. In both cases, it has been proposed that the hydrogen bonding network is responsible for their extremely low oxygen dissociation rates (15, 41). Despite this analogy, the oxygen dissociation rate constant for HbII$_{LP}$ and Hb$_{Asc}$ shows a difference of 2 orders of magnitude (0.11 and 0.004 s^{-1}, respectively). This suggests that other factors, like the His[97](F8) trans-effect and its orientation, could play an important role in determining this rate difference. The resonance Raman measurements allows a comparison between the Fe-His stretching mode of Mb, HbII$_{LP}$, and Hb$_{Asc}$, at 220, 211, and 202 cm^{-1}, respectively, whereas for recombinant HbI$_{LP}$ and the HbI$_{LP}$Phe(B10) $\rightarrow$ Tyr mutant, the Fe-N stretching mode is characterized by a band at 219 cm^{-1} (Fig. 4). The Fe-His normal mode falls into the group of heme proteins that have a neutral proximal histidine, characteristic of those responsible for transporting oxygen, where the proximal histidine environment differs for these three hemeproteins. The strength of the
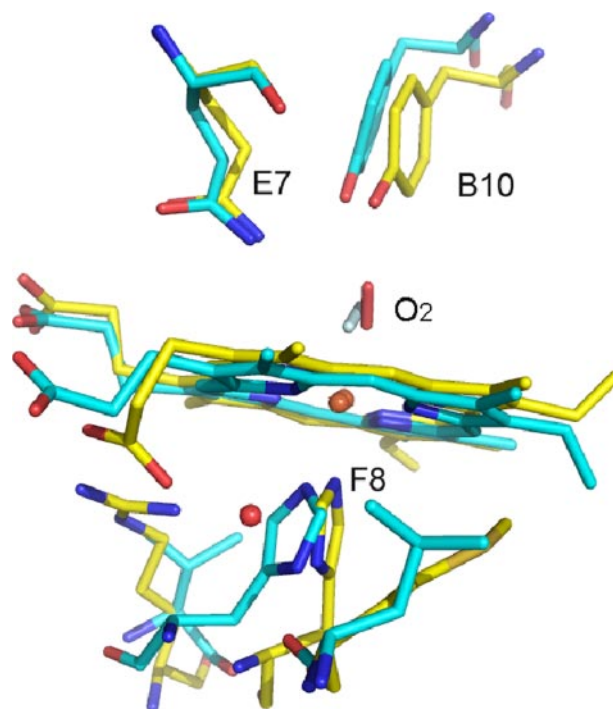
FIGURE 6. **Oxygen heme moiety.** Least square superposition of HbII$_{LP}$ (*yellow*) and Hb$_{Asc}$ (*cyan*, PDB code 1ASH). The superposition was carried out taking into account all the residues in the structure (amino acids and prosthetic group). The water molecule forming a hydrogen bond between the propionate group and His[97](F8) in HbII$_{LP}$ is also shown. This water molecule is not present in the oxygen bound structure of Hb$_{Asc}$. The oxygen molecule shows opposite orientation in both structures (the oxygen molecule in Hb$_{Asc}$ is shown in *clear cyan*).

hydrogen bond formed by a nitrogen proton in the proximal histidine and the polarity of the environment are powerful factors for determining the Fe-His stretching frequency in the heme-histidine moiety. This hydrogen bonding network in hemoglobins and myoglobins has also been also related to ligand affinity (37, 40). The significant differences observed in the heme-ligand dissociation rate constants between Mb and Hb$_{Asc}$ have mainly been attributed to the tilted orientation of the His(F8) with regard to the pyrrole rings of the heme (45). Fig. 6 shows an overlay of the oxy heme moiety of Hb$_{Asc}$ and HbII$_{LP}$ indicating several structural differences in the orientation of the proximal histidine, the bound oxygen, propionates, and vinyl groups. In particular, the presence of a water molecule between the propionate group of heme and His(F8) in HbII$_{LP}$ suggests that the Fe-His strength and the His-Fe trans-effect may be modulated by this hydrogen bond. Furthermore, the orientation of His(F8), as suggested for Hb$_{Asc}$, can also contribute to the observed Fe-His frequency. The combination of these factors facilitates the strength of the Fe-O$_2$ complex in the distal heme pocket. Moreover, the small distal cavity volume of HbII$_{LP}$ and its hydrogen bonding network with the heme-O$_2$ moiety is consistent with the relationship between the Fe-O$_2$ stretching mode and its oxygen dissociation rate constant (k_{off}) (46). This is supported by data in Table 3, which shows a rough inverse relationship between these two properties for HbII$_{LP}$, HbI$_{LP}$, and several HbI$_{LP}$ mutants. For example, oxyHbII$_{LP}$ and oxyHbI$_{LP}$ show Fe-O frequencies at 572 and 567 cm^{-1} correlated with an oxygen dissociation rate constant (2) of 0.11 and

TABLE 3

vFe-O$_2$ and dissociation rate constants (k_{off}) for HbII$_{Lp}$, HbI$_{Lp}$, and HbI$_{Lp}$ mutants

Heme protein	v_{FeO_2}	k_{off}
	cm^{-1}	s^{-1}
HbI (Gln(E7), Phe(B10), Phe(E11))	567	61.0[a]
HbI$_r$ (Gln(E7), Phe(B10), Phe(E11))	567	140.0
HbIGln(E7) → Val	563	500.0
HbIGln(E7) → Asp	563	375.0
HbIGln(E7) → His	569	3.0
HbIPhe(B10) → Tyr	571	0.60
HbII (Gln(E7), Tyr(B10), Phe(E11))	572	0.11[a]

[a] From Ref. 2.

61 s^{-1}, respectively. Similarly, HbI$_{Lp}$Gln(E7) → Asp and HbI$_{Lp}$Gln(E7) → Val mutants show an increase in the dissociation rate constant from 140 s^{-1} (for HbIr specie) to 375 and 500 s^{-1}, whereas the Fe-O normal mode frequency decreases to 563 cm^{-1} (46). The faster oxygen dissociation rates suggest that the interactions of the E7 residue in these two mutants are much weaker than in HbI$_{Lp}$, thus corroborating that the absence of a hydrogen bond induces a lower Fe-O vibrational frequency. Although no dipolar interaction exists between the residues in the E7 position in these two mutants, the observed frequencies in the HbI$_{Lp}$ mutants are higher than expected probably due to multipole interactions of the three phenylalanine residues (B10, E11, and CD1) in the distal side of the heme (47). The HbI$_{Lp}$Gln(E7) → His mutant induces a much stronger polar interaction between this residue and the dioxygen heme complex with a dissociation rate constant (k_{off}) of 3 s^{-1}, suggesting the presence of dipolar interactions with the His(E7) center. This is consistent with the increase in the Fe-O energy and the kinetics studies on Mb, which indicated that the hydrogen bond between His(E7) and the oxygen coordinated to the iron control the k_{off} rate. The Tyr(B10) in the HbI$_{Lp}$Phe(B10) → Tyr mutant and in HbII$_{Lp}$ is also stabilizing the coordinated dioxygen molecule as evidenced by the increase in the frequency from 567 to 571 cm^{-1}, and to 572 cm^{-1}, respectively, and the decrease in their dissociation rate constants from 61 to 0.6 s^{-1}, and to 0.11 s^{-1}, respectively. As mentioned above, despite similarities in their hydrogen bonding network, Hb$_{Asc}$ and HbII$_{Lp}$ show significantly different oxygen dissociation rate constants (0.0041 and 0.11 s^{-1}, respectively) (2, 48). Moreover, the Hb$_{Asc}$ show a Fe-His normal mode at 202 cm^{-1}, whereas for HbII$_{Lp}$ this frequency is present at 211 cm^{-1}. Thus, differences in the His(F8) trans-effect and the orientation of the oxygen molecule in the oxyHbII$_{Lp}$ and oxyHb$_{Asc}$ complexes (Fig. 6) must have an important role to explain the observed experimental data. Similarly, this is also supported by studies of CO complexes showing three different conformers at 1912, 1956, and 1965 cm^{-1} for Hb$_{Asc}$-CO, whereas the HbII$_{Lp}$-CO complex show only the presence of the A$_3$ and A$_0$ conformers at 1924 and 1964 cm^{-1} in the infrared spectra (15, 46). Therefore, the interplay between the small HbII$_{Lp}$ heme pocket structure, the hydrogen bonding network to the proximal and distal heme environments, the His(F8) trans-effect, and the orientation of the oxygen molecule in the oxy complex are responsible for the stability of the oxyHbII$_{Lp}$ complex.

In truncated hemoglobins (trHbs), the oxy trHb complex shows, in general, a much lower energy for the Fe-O vibrational mode (542–560 cm^{-1}) than Mb (49), HbI$_{Lp}$, and HbII$_{Lp}$. Moreover, oxy trHbs tend to present an inverse correlation between the Fe-O frequency and the oxygen dissociation rate, similarly for oxyHbI$_{Lp}$ and oxyHbII$_{Lp}$ there is apparently also a rough inverse relationship with the dissociation constants but their Fe-O frequency is present at higher energy (567–572 cm^{-1}). The fact that trHbs have a hydrogen bonding network interacting with the proximal and distal oxygens of the heme-O$_2$ moiety, whereas HbI$_{Lp}$ and HbII$_{Lp}$ present a hydrogen bonding network interacting only with the distal oxygen of the oxyheme complex may account for the observed trend. Particularly, the Fe$^{\delta+}$-O-O$^{\delta-}$ center is highly polar (50) and the formation of hydrogen bonding between heme pocket amino acids and one or both oxygens of the oxyheme complex can generate different moiety resonance structures. Furthermore, because the low frequency Fe-O Raman active vibrational mode arises from the interactions between the stretch and bend motion of Fe$^{\delta+}$-O-O$^{\delta-}$, at equilibrium, an approximate potential leading to the Fe-O vibrational frequency can be expressed as Equation 1,

$$V = f_1\Delta r_1{}^2 + f_2\Phi\Delta r_2{}^2 \pm f_1 f_2 \Delta r_1 \Delta r_2 + f_\Phi \Delta \Phi^2$$
$$\pm f_1 f_\Phi \Delta r_1 \Delta \Phi \pm f_2 f_\Phi \Delta r_2 \Delta \Phi \quad \text{(Eq. 1)}$$

where f_1, f_2, $f_{\hat{O}}$, r_1, r_2, and $\hat{O}$ are the force constant and geometries for the Fe-O, O-O, and Fe-O-O atoms, respectively. Similarly, $f_1 f_2$, $f_1 f_{\hat{O}}$, and $f_2 f_{\hat{O}}$ are the associated interaction force constants, and their signs can be positive or negative (51, 52) depending on the Fe$^{\delta+}$-O-O$^{\delta-}$ resonance structures, geometry, and central atom hybridization, which in turn are affected by the hydrogen bonding network present in the oxyhemoglobin species. It is plausible that the combination and magnitude of the sign in these coupling constants may be responsible for the lack of a single correlation between the Fe-O frequency and the hemeproteins oxygen dissociation constant.

Factors Influencing HbII$_{Lp}$ Oxygen Selection—Different roles have been suggested for the hemoglobin variants of *L. pectinata* (1, 3). HbI$_{Lp}$ is a sulfide-reactive monomeric protein, whereas HbII$_{Lp}$ and HbIII$_{Lp}$ are responsible for the oxygen transport and remain unaffected by the presence of H$_2$S. The factors underlying this unique behavior and ligand selection between HbI$_{Lp}$ and HbII$_{Lp}$/HbIII$_{Lp}$ clearly depend on the heme iron oxidation state; however, the mechanism underlying the deoxy heme stability in HbII$_{Lp}$ is still unknown. *In vitro* HbI$_{Lp}$ and HbII$_{Lp}$ bind oxygen with an association rate constant of 100–200 × 10^6 and 0.39 × 10^6 M^{-1} s^{-1}, and hydrogen sulfide with association rate constant values of 226 × 10^3 and 11.3 × 10^3 M^{-1} s^{-1}, respectively (2, 3). This indicates that HbI$_{Lp}$ binds both ligands much faster than HbII$_{Lp}$. Similar to HbII$_{Lp}$, kinetic analysis of the HbI$_{Lp}$Phe(B10) → Tyr mutant with O$_2$ and H$_2$S indicates that in this variant the association constant of both ligands decreases to 6.8 × 10^6 and 3.37 × 10^3 M^{-1} s^{-1}, respectively, when compared with HbI$_{Lp}$. Furthermore, the H$_2$S dissociation constant for HbII$_{Lp}$, rHbI$_{Lp}$, and the HbI$_{Lp}$Phe(B10) → Tyr mutants are 17 × 10^{-3}, 0.04 × 10^{-3}, and 0.06 × 10^{-3} s^{-1}, respectively, whereas for the oxygen species these values are 0.11, 140, and 0.6 s^{-1}, respectively. Thus, the data indicate that in HbI$_{Lp}$ the Phe(B10) → Tyr mutation cannot account for the

properties of HbII$_{Lp}$-SH$_2$ complex reactivity but it can explain the smaller dissociation constant of oxyHbII$_{Lp}$. Replacing Phe(B10) by Tyr in the HbI$_{Lp}$Phe(B10) $\rightarrow$ Tyr mutant may decrease the size of the HbI$_{Lp}$ heme cavity, thus causing a reduction in ligand association. Independently of the heme iron oxidation state driving force for the selection of O$_2$ or H$_2$S, the heme cavity of HbII$_{Lp}$ is smaller (872 Å^3) than the HbI$_{Lp}$. Dynamic features in HbI$_{Lp}$, Mb, and triple Mb mutant (L29F/H64Q/V68F) revealed a large cavity, suggesting that the larger cavities favor the binding of H$_2$S by HbI$_{Lp}$ (43). The reduction of the heme cavity of both HbII$_{Lp}$ and HbI$_{Lp}$Phe(B10) $\rightarrow$ Tyr may help to stabilize the Fe^{II}-O$_2$ moiety once O$_2$ binds the heme iron center by forming hydrogen bonding interactions with Gln(E7) and Tyr(B10) as evidenced by the resonance Raman and oxygen off rate analyses presented above. Moreover, the reduction of the heme cavities in both proteins, caused in part by Tyr(B10), may help prevent oxidation of the ferrous iron center by impeding access of external water molecules into the distal environment. Indeed, a direct role of Tyr(B10) in preventing oxidation of Fe^{II} as well as ligand selection can be observed in the pH titration analysis of HbI$_{Lp}$, HbI$_{Lp}$Phe(B10) $\rightarrow$ Tyr, and HbII$_{Lp}$. The data showed that the high affinity of HbII$_{Lp}$ and the HbI$_{Lp}$Phe(B10) $\rightarrow$ Tyr mutant for oxygen is pH-dependent. Similarly, a decrease from pH 7.5 to 5.5 was necessary to fully oxidize both HbII$_{Lp}$ and the HbI$_{Lp}$Phe(B10) $\rightarrow$ Tyr mutant, suggesting that the tyrosine plays an important role in regulating the oxidation of the heme group. Previous experiments has been suggested a relationship between the pK_a values of the ionizable groups associated with the heme and the role of the hydrogen bonding interactions on the heme oxygen dissociation rate (53). Furthermore, for met-aquo HbII$_{Lp}$ and HbI$_{Lp}$Phe(B10) $\rightarrow$ Tyr, the UV-visible pH data shows, at neutral conditions, bands at 486, 541, 577, and 603 nm for both proteins. This suggests the existence of an open and closed conformation due to the interactions in the coordination of the Tyr(B10)(OH) and the ligand, to the heme iron. This means that, in the open conformation the Tyr^{30}(B10) swings away from the iron, whereas in the closed conformation remains at very close distance and may interact with the ligand (47).

Overall, the data suggest a model for the *in vivo* mechanism of the clam *L. pectinata* where the function of HbII$_{Lp}$ to bind and possibly transport oxygen to the host bacteria is regulated by the dynamic displacements of the Gln^{65}(E7) and Tyr^{30}(B10) pair toward the heme to protect it from the change in the heme oxidation state from Fe^{II} to Fe^{III}. This suggested mechanism avoids the binding of H$_2$S to HbII$_{Lp}$ that disrupts its function of oxygen transport in an environment rich in hydrogen sulfide. In summary, the results from the crystallographic data show that a small heme pocket cavity for HbII$_{Lp}$ induces the formation of strong hydrogen bonds between the iron and oxygen molecule. Resonance Raman data supports the existence of a hydrogen bonding network between Gln(E7) and Tyr(B10) that stabilizes the binding of the oxygen to HbII$_{Lp}$ complex shown in Fig. 3. This, together with the proximal histidine trans-effect, and the pH dependence of the oxidation state substantiates the role of HbII$_{Lp}$ in controlling the oxygen dissociation rate.

REFERENCES

1. Read, K. R. (1965) *Comp. Biochem. Physiol.* **15,** 137–157
2. Kraus, D. W., and Wittenberg, J. B. (1990) *J. Biol. Chem.* **265,** 16043–16053
3. Kraus, D. W., Wittenberg, J. B., Lu, J. F., and Peisach, J. (1990) *J. Biol. Chem.* **265,** 16054–16059
4. Rizzi, M., Wittenberg, J. B., Coda, A., Fasano, M., Ascenzi, P., and Bolognesi, M. (1994) *J. Mol. Biol.* **244,** 86–99
5. Bolognesi, M., Rosano, C., Losso, R., Borassi, A., Rizzi, M., Wittenberg, J. B., Boffi, A., and Ascenzi, P. (1999) *Biophys. J.* **77,** 1093–1099
6. Rizzi, M., Wittenberg, J. B., Coda, A., Ascenzi, P., and Bolognesi, M. (1996) *J. Mol. Biol.* **258,** 1–5
7. Hockenhull-Johnson, J. D., Stern, M. S., Martin, P., Dass, C., Desidero, D. M., Wittenberg, J. B., Vinogradov, S. N., and Walz, D. A. (1991) *J. Protein Chem.* **10,** 609–622
8. Torres, E., Renta, J. Y., Rodríguez, Y., López-Garriga, J., and Cadilla, C. L. (2003) *J. Protein Chem.* **22,** 683–690
9. Pietri, R., Granell, L., Cruz, A., De Jesús, W., Lewis, A., León, R., Cadilla, C. L., and López Garriga, J. (2005) *Biochim. Biophys. Acta* **1747,** 195–203
10. Yang, J., Kloek, A. P., Goldberg, D. E., and Mathews, F. S. (1995) *Proc. Natl. Acad. Sci. U. S. A.* **92,** 4224–4228
11. Couture, M., Yeh, S., Wittenberg, B. A., Wittenberg, J. B., Ouellet, Y., Rousseau, D. L., and Guertin, M. (1999) *Proc. Natl. Acad. Sci. U. S. A.* **96,** 11223–11228
12. Milani, M., Pesce, A., Ouellet, Y., Ascenzi, P., Guertin, M., and Bolognesi, M., (2001) *EMBO J.* **20,** 3902–3909
13. Condon, P. J., and Royer, W. E., Jr. (1994) *J. Biol. Chem.* **269,** 25259–25267
14. Royer, W. E., Jr., Heard, K. S., Harrington, D. J., and Chiancone, E. (1995) *J. Mol. Biol.* **253,** 168–186
15. Peterson, E. S., Huang, S., Wang, J., Miller, L. M., Vidugiris, G., Kloek, A. P., Goldberg, D. E., Chance, M. R., Wittenberg, J. B., and Friedman, J. M. (1997) *Biochemistry* **36,** 13110–13121
16. De Jesús-Bonilla, W., Jia, Y., Alayash, A. I., and López Garriga, J. (2007) *Biochemistry* **46,** 10451–10460
17. De Jesús-Bonilla, W., Cruz, A. Lewis, A., Cerda, J., Bacelo, D. E., Cadilla, C. L., and López-Garriga, J. (2006) *J. Biol. Inorg. Chem.* **11,** 334–342
18. León, R. G., Munier-Lehmann, H., Barzu, O., Baudin-Creuza, V., Pietri, R., López-Garriga, J., and Cadilla, C. L. (2004) *Protein Expr. Purif.* **38,** 184–195
19. Altschul, S. F., Madden, T. L., Schäffer, A. A., Zhang, J., Zhang, Z., Miller, W., and Lipman, D. J. (1997) *Nucleic Acids Res.* **25,** 3389–3402
20. Thompson, J. D., Higgins, D. G., and Gibson, T. J. (1994) *Nucleic Acids Res.* **22,** 4673–4680
21. Gavira, J. A., De Jesús, W., Camara-Artigas, A., Lopez-Garriga, J., and Garcia-Ruiz, J. M. (2006) *Acta Crystallogr. Sect. F Struct. Biol. Crystallogr. Commun.* **62,** 196–199
22. García-Ruiz, J. M. (2003) *Methods Enzymol.* **368,** 130–154
23. Otwinowski, Z., and Minor, W. (1997) *Methods Enzymol.* **276,** 307–326
24. Brunger, A. T., Adams, P. D., Clore, G. M., Delano, W. L., Gros, P., Grosse-Kunstleve, R. W., Jiang, J. S., Kuszewski, J., Nilges, M., Pannu, N. S., Read, R. J., Rice, L. M., Simonson, T., and Warren, G. L. (1998) *Acta Crystallogr. Sect. D Biol. Crystallogr.* **54,** 905–921
25. Bailey, S. (1994) *Acta Crystallogr. Sect. D Biol. Crystallogr.* **50,** 760–763
26. Emsley, P., and Cowtan, K. (2004) *Acta Crystallogr. Sect. D Biol. Crystallogr.* **60,** 2126–2132
27. Winn, M. D., Isupov, M. N., and Murshudov, G. N. (2001) *Acta Crystallogr. Sect. D Biol. Crystallogr.* **57,** 122–133
28. Lovell, S. C., Davis, I. W., Adrendall, W. B., III, de Bakker, P. I., Word, J. M., Prisant, M. G., Richardson, J. S., and Richardson, D. C. (2003) *Proteins* **50,** 437–450
29. Laskowski, R. A., MacArthur, M. W., Moss, D. S., and Thornton, J. M. (1993) *J. Appl. Crystallogr.* **26,** 283–291
30. Frishman, D., and Argos, P. (1995) *Proteins* **23,** 566–579
31. Hutchinson, E. G., and Thornton, J. M. (1996) *Protein Sci.* **5,** 212–220
32. Kabsch, W. (1976) *Acta Crystallogr. Sect. A* **32,** 922–923
33. Krissinel, E., and Henrick, K. (2005) *Comput. Life Sci. Proc.* **3695,** 163–174
34. Hubbard, S. J., and Thornton, J. M. (1993) *NACCESS, Computer Program*, Department of Biochemistry and Molecular Biology, University College, London

35. Binkowski, T. A., Naghibzadeh, S., and Liang, J. (2003) *Nucleic Acids Res.* **31,** 3352–3355

36. Royer, W. E., Knapp, J. E., Strand, K., and Heaslet, H. A. (2001) *Trends Biochem. Sci* **26,** 297–304

37. Smerdon, S. J., Krzywda, S., Wilkinson, A. J., Brantley, R. E., Carver, T. E., Hargrove, M. S., and Olson, J. S. (1993) *Biochemistry* **32,** 5132–5138

38. Royer, W. E., Jr., Pardanani, A., Gibson, Q. H., Peterson, E. S., and Friedman, J. M. (1996) *Proc. Natl. Acad. Sci. U. S. A.* **93,** 14526–14531

39. Pardanani, A., Gambacurta, A., Ascoli, F., and Royer, W. E. (1998) *J. Mol. Biol.* **284,** 729–739

40. Carver, T. E., Brantley, R. E., Jr., Singleton, E. W., Arduini, R. M., Quillin, M. L., Phillips, G. N., Jr., and Olson, J. S. (1992) *J. Biol. Chem.* **267,** 14443–14450

41. Cerda, J., Echevarría, Y., Morales, E., and López-Garriga, J. (1999) *Biospectroscopy* **5,** 289–301

42. Mukai, M., Mills, C. E., Poole, R. K., and Yeh, S. R. (2001) *J. Biol. Chem.* **276,** 7272–7277

43. Fernández-Alberti, S., Bacelo, D. E., Binning, R. C., Echave, J., Chergui, M., and Lopez-Garriga, J., (2006) *Biophys. J.* **91,** 1698–1709

44. Zhou, Y. Q., Zhou, H. Y., and Karplus, M. (2003) *J. Mol. Biol.* **326,** 593–606

45. Das, K. T., Boffi, A., Chiancone, E., and Rousseau, A. D. (1999) *J. Biol. Chem.* **274,** 2916–2919

46. Pietri, R., Granell, L. B., León, R., Cadilla, C. L., and López-Garriga, J. (2006) *Biochim. Biophys. Acta* **1764,** 758–765

47. Navarro, A., Maldonado, M., González-Lagoa, J., López, R., López-Garriga, J., and Colón, J. (1996) *Inorg. Chim. Acta* **243,** 161–166

48. Blaxter, M. L., Vanfleteren, J. R., Xia, J., and Moens, L. (1994) *J. Biol. Chem.* **269,** 30181–30186

49. Lu, C., Egawa, T., Wainwright, L. M., Poole, R. K., and Yeh, S.-R. (2007) *J. Biol. Chem.* **282,** 13627–13636

50. Hirota, S., Li, T., Phillips, G. H., Olson, J. S., Mukai, M., and Kitagawa, T. (1996) *J. Am. Chem. Soc.* **118,** 7845–7846

51. Coulson, C. A., Duchesne, J., and Manneback, C. (1947) *Nature* **159,** 794–795

52. Califano, S. (1976) *Vibrational States*, pp. 95–97, John Wiley & Sons, New York

53. Saroff, H. A. (2004) *J. Theor. Biol.* **229,** 113–118